

Train Track Misalignment Detection System

By

Kang Chun Hong

13835

Dissertation submitted in partial fulfilment of

the requirements for the

Bachelor of Engineering (Hons)

(Electrical & Electronics Engineering)

MAY 2014

Universiti Teknologi PETRONAS

Bandar Seri Iskandar

31750 Tronoh

Perak Darul Ridzuan

CERTIFICATION OF APPROVAL

Train Track Misalignment Detection System

By

Kang Chun Hong

13835

A project dissertation submitted to the
Electrical & Electronics Engineering Programme
Universiti Teknologi PETRONAS
in partial fulfillment of the requirement for the
BACHELOR OF ENGINEERING (Hons)
(ELECTRICAL AND ELECTRONICS)

Approved by,

(Mr. Abu Bakar Sayuti bin Hj Mohd Saman)

UNIVERSITI TEKNOLOGI PETRONAS

TRONOH, PERAK

MAY 2014

CERTIFICATION OF ORIGINALITY

This is to certify that I am responsible for the work submitted in this project, that the original work is my own except as specified in the references and acknowledgements, and that the original work contained herein have not been undertaken or done by unspecified sources or persons.

KANG CHUN HONG

ABSTRACT

A feasible, portable and low-cost detection technique for train track misalignment was proposed. Currently, the detection of orientation movement of train along a flat head rail focuses on using different combination of optical sensor, accelerometer and gyro sensors, separated at several compartment and parts of the train. However, due to high implementation cost and complexity, these systems could not be widely implemented in all of the passenger-loaded compartments train and not suitable to switch from one platform to another, as it requires complex mounted installations. Hence, a MEMS-based Inertia Measurement Unit (IMU) was proposed to be implemented as an alternative low-cost and portable detection solution. The primary objective focuses on identifying potential misaligned track section through tri-axis Euler angles and tri-axis acceleration of the train. Equipped with an onboard Arduino ATmega328 microcontroller, the IMU was programmed through Arduino IDE by using USB-to-UART converter. Direction-cosine-matrix (DCM) algorithm was also implemented to detect and correct numerical error for the gyroscope via reference data from accelerometer. Practical implementation had also being conducted on both car and passenger-loaded train. These data were extracted onto PC for storage and post-processing via MATLAB. The measurements were analyzed and presented with discussion on track characteristics, train motion and noise. Also, analysis through the frequency spectrum over time provides insight onto possible misalignment region. The overall measurement analysis showed good correlation between actual track features and IMU sensor data.

ACKNOWLEDGEMENT

First and foremost, I would like to express special credit and deepest appreciation to my supervisor, Mr. Abu Bakar Sayuti and co-supervisor, Assc. Prof. Dr. Fawnizu Azmadi Hussin for their continuous support and guidance throughout the project. They have always been helpful, caring and continuously supporting me on exploring this new field of research. Also, the collaborative environment in UTP allowed me to interact with researchers and lecturers from various disciplines. My sincere appreciation also goes to Mr. Patrick Sebastian and Dr. Mohd Zuki for providing and sharing their opinion on this project. I would also like to express my earnest thank-you to all the academic members and management of UTP Electrical and Electronics Engineering Department for continually and convincingly conveyed a spirit of caring in regard to teaching and learning in the past four years. Finally, I thank my lovely family and friends for their unlimited caring and support.

TABLE OF CONTENTS

CERTIFICATION OF APPROVAL	i
CERTIFICATION OF ORIGINALITY	ii
ABSTRACT	iii
ACKNOWLEDGEMENT	iv
CHAPTER 1: INTRODUCTION	
1.1 Background	1
1.2 Problem Statement	1
1.3 Objectives and Scope of Study	2
CHAPTER 2: LITERATURE REVIEW	
2.1 Track Misalignment Detection System	3
2.2 Tilting Concept	5
2.3 Inertia Measurement System	6
CHAPTER 3: METHODOLOGY	
3.1 Overview	8
3.2 Experimental Setup	9
3.3 Hardware Setup	11
3.4 Hardware-Software Interface	12
3.5 Direction-Cosine-Matrix (DCM) Algorithm	14
CHAPTER 4: RESULTS AND DISCUSSIONS	
4.1 Output Data	17
4.2 Car-mounted Field Testing	20
4.3 Train-mounted Field Testing	26
4.3.1 Overall Measurement Analysis	28
4.3.2 Track Characteristics	29
4.3.3 Frequency Spectrum	31
CHAPTER 5: CONCLUSIONS AND RECOMMENDATIONS	
5.1 Conclusion	35
5.2 Recommendations	36
REFERENCES	37

LIST OF FIGURES

Figure 1. An example of TRC used in Network Rail, UK, which utilizes optical sensor to measure longitudinal level and track irregularities -----	4
Figure 2. The tilting train (right) was designed to compensate the lateral forces experienced by the vehicles with a certain angle of tilting, as compared to a non-tilting train (left) -----	5
Figure 3. Illustration of axis orientation on train -----	8
Figure 4. Simple flow diagram on the overall setup of the project -----	9
Figure 5. Key Milestones of this project -----	9
Figure 6. Connection between Arduino IMU and USB-UART Converter -----	11
Figure 7. An example of analog data from gyroscope and accelerometer shown on serial monitor -----	12
Figure 8. Program flowchart representing the workflow of interfacing between PC and IMU -----	13
Figure 9. Block diagram of direction-cosine-matrix (DCM) algorithm -----	14
Figure 10. Uncorrected and corrected output data when IMU placed on a reasonably flat surface -----	17
Figure 11. Uncorrected and corrected output data when IMU rotate to approximately 45° along x-axis -----	18
Figure 12. Uncorrected and corrected output data when IMU rotate to approximately 45° along y-axis -----	19
Figure 13. One of the bump as located in front of Chancellor Hall, UTP -----	20
Figure 14. Display of measurement data on serial window -----	21
Figure 15. Measurement data in Text format -----	21
Figure 16. Measurement data in Excel file -----	22
Figure 17. Collected IMU data for car-mounted field testing over distance -----	23
Figure 18. Close-up on pitch angle, x-axis acceleration and z-axis acceleration as car passes through second bump -----	24
Figure 19. Collected IMU data with filtering for car-mounted field testing -----	25
Figure 20. Collected IMU data for train-mounted field testing, covering from Kampar Station to KL Sentral Station -----	27

Figure 21. Distance coverage for train-mounted field testing. Picture inset shows the mounting of prototype on-board -----	28
Figure 22. Vertical acceleration measurement in KM147.6 to KM148 -----	29
Figure 23. Roll angle measurement data corresponding to two banked curvature -	31
Figure 24. Frequency spectrum over time of y-axis acceleration -----	31
Figure 25. Frequency spectrum over time of z-axis acceleration -----	32
Figure 26. Frequency spectrum over time of roll angle -----	33
Figure 27. Frequency spectrum over time of pitch angle -----	33

LIST OF TABLES

Table 1. Gantt Chart of the project -----	10
Table 2. Connection table between ArduIMU and USB-UART Converter -----	12

CHAPTER 1

INTRODUCTION

1.1 Background

Since the late 18th century, introduction of railway-guided vehicles have improved personal mobility and ease communication between different places. Even until today's modern world, majority of countries still relying on railway vehicles as the major medium of transportation, which includes different types of train services, such as freight train, inter-city trains, high speed train, trams and mine lines. All these railway vehicles share the common characteristics, where they are guided by a rail system. Some example of railway includes common railway, electrified railway, high-speed rail, maglev and monorail [1]. As the railway vehicle need to be operated on a guided pathway, the train operator only has the control over the longitudinal direction of the train by changing its speed, but no any direct control over the horizontal, orientation or other movement of the train. Hence, any poorly maintained, misaligned and faulty railway track could results in vast orientation on the train, which could eventually lead to discomfort or motion sickness by the passengers. Some of the serious cases could even lead to derailment and rollover by the train.

1.2 Problem Statement

In order to effectively detect any misalignment and faulty tracking system along the railway, several methods had been proposed and patented in the U.S., which includes detection of changes in the RF signals or sonic vibration along the train track [2-3]. However, most of these methods often required a huge number of expensive instruments to be installed at various site of investigation. Also, the current system used in most of the European Countries often requires multiple sensors to be installed in various compartment of the train. Hence, these highly complex systems could require high installation costs and not portable to be switch to other platform. It will also require a Track Recording Coaches (TRC) or a test drive to run on the track after maintenance work had being conducted.

Hence, it might incur more cost and the actual orientation movement between a passenger-loaded train and railway could not be provided. As the misaligned track are often caused by heating and stress effect, the train track might possibly being affected by any weather changes within a short period of time, especially during the summer, even after regular track maintenance had being conducted.

1.3 Objectives and Scope of Study

The purpose of this study is to develop a train track misalignment detection system with a sensitive measurement sensor unit interface onto a microcontroller-based device, where it will provide actual readings and data with respect to the movement profile of the train. From which, the measurement data collected from an actual train will be able to provide valuable information for the train operator to detect any faulty train track and improves response of railway vehicles with regards to the track condition.

The term ‘misalignment’ in this project refers to out of adjustment of horizontal and vertical layouts of railing system. It generally describes the straightness or uniformity of the track along a certain distance. A number of causes of misalignment due to track geometry defect include various mechanical failures of track components, such as ballast, dipped joints, lateral panel shift and faulty switching gear. This project aims to be implemented on conventional system, such as railways and tramways, while other guided system such as monorails and magnetic levitation will not be considered predominantly, as they have different track conditions. The primary objectives of this study are:

- To identify suitable measurement sensor for detection of orientation movement on railway vehicles.
- To design, build and interface a sensitive measurement unit onto a microcontroller-based device and PC.
- To implement and verify the feasibility of designed prototype on train motion measurement.
- To display, interpret and analyze collected data on a single software platform.

CHAPTER 2

LITERATURE REVIEW

2.1 Track Misalignment Detection System

The development of train track misalignment detection started in the 70s, as one of the early inventions on this scope of study was patented in 1972, where they used a transmitter to provide coded pulse signals and produce electrical energy in different site of the train track [12]. Any substantial changes in the transmitted signals will be detected by a receiver placed at another end point. In between 1980 to 1990, another three patents were filed in United States. These three patents implied single radio frequency, dual frequency signals and sonic vibration, respectively onto the train track [2, 3, 14]. Any changes substantial changes along the track, such as phase angle and impedance were detected by another receiver placed at a potential misalignment site. These collected signals and measurement were also being compared to a set of pre-determined values.

However, Theodore R. Anderson pointed out that these measurement systems often required a huge amount of installation cost to purchase equipment and consumes a lot of man power and time [15]. These patents showed a significant improvement on the detection of major misaligned track, however they were not capable of detecting minor faulty train track, especially at the connection point of bridges and train track [2, 14-15]. Some of the track built on bridges might disconnect or not properly aligned with the tracks on the land during the event of railway vehicles passing through bridges. Until the early 2000s, another patent was filed in regards for detecting misaligned railroad tracks. An RF generator was used to imply energy onto railway tracks. Any faulty train track will induces a certain amount of energy, which are detectable by an antenna and thus trigger a safety alarm system [15].

After the first few years of 2000s, the continuous research and development on the detection technique for train track misalignment managed to produce a number of effective systems that currently being implemented, especially in the

European Countries. According to a collaborative report recently published by International Union of Railways (UIC) in July 2013, Track Recording Coaches (TRC) was commonly used in Switzerland, Sweden and the UK [16]. Performed under loaded condition, the track geometry measurements in Switzerland were collected by an opto-inertial track geometry measurement system, where it utilizes six optical sensor boxes placed under the train compartment to collect track profile and determine any irregularities along the railway. Also in Switzerland, Infranord uses measurement vehicles with accelerometer and Linear Variable Differential Transformers (LVDT) placed under the compartment to measure the quality of railway [12, 16]. Meanwhile, for the TRC in the UK as shown in Figure 1, a combination of 3-axis accelerometer, gyro sensor and optical sensor placed separately in the train were used to detect fault or broken railway [16]. Typically, all these measurement systems could detect defects along the railway in the speed up to 300km/h, with a sampling rate between 50 – 250 mm [12, 16].

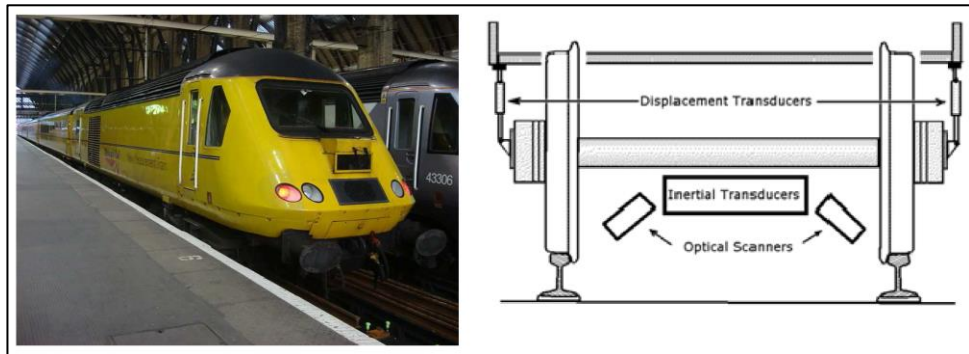


Figure 1. An example of TRC used in Network Rail, UK, which utilizes optical sensor to measure longitudinal level and track irregularities [16].

Another method of measurement was called the Continuous Track Monitoring (CTM) system. This system was used by the Deutsche Bahn, a German railway company, where several accelerometers were installed in different parts of the train, mainly closed to axle bearing of the train compartment [16-17]. In addition to that, a GPS mapping technique and 6-Degree of Freedom (DOF) inertia measurement unit was also being employed to collect measurement data along with its location tag [12, 16-18]. Despite different methods of data collection along the railway, most of the measurement systems shared a common

characteristic, where the collected data have to be sent and stored onto a private system server, ranging from a weekly to yearly basis [12, 16]. From which, the maintenance team will be able to post-process and analyze the data, while further improves maintenance management via systematic monitoring on track profile.

2.2 Tilting Concept

When a railway vehicle moves along its longitudinal direction along the track, the irregularities of roadway exert a number of components of acceleration, including vibration from faulty track components acting upon the train. These forces, together with the classical track hunting oscillation caused the swaying motion on the train [4]. A study by Rickard Persson pointed out that when a train experiences irregular orientation or making a sharp curve, the train body will tilt to a certain angle, but with its body still mainly attached to the train track [5]. This concept was also being applied to the invention of tilting train, where the train tilt inwards to compensate the centrifugal force when making pass through a curves [5-6]. Figure 2 shows the tilting train moves inwards to reduce the lateral forces. It helps to enhanced turning speed while maintaining a smooth transition during banked curvature.

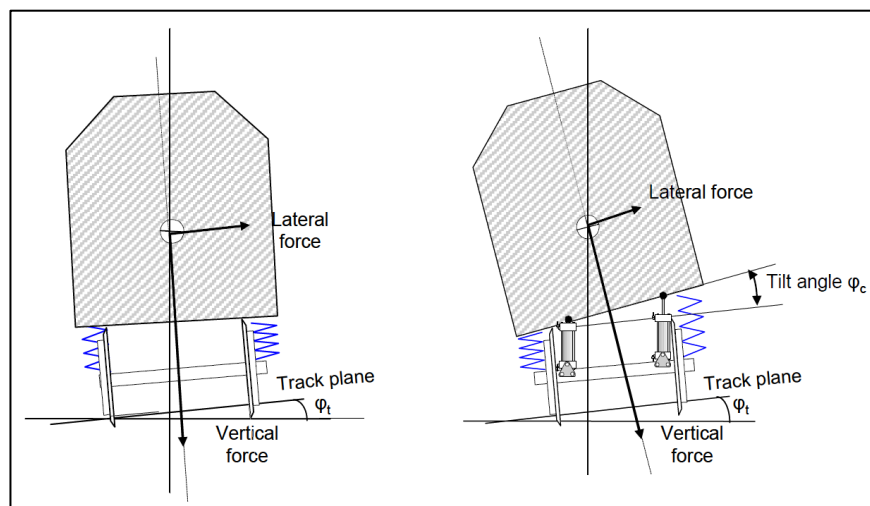


Figure 2. The tilting train (right) was designed to compensate the lateral forces experienced by the vehicles with a certain angle of tilting, as compared to a non-tilting train (left) [5].

Hence, an effective tilting measurement system is required to measure the allowable tilting angle. An actively tilted train uses computer-controlled mechanism with sensor to measure and control the tilting angle with an electric and hydraulic actuator [5, 7]. One of the most successful actively tilted train is Pendolino Tilting Train operating in 11 countries across Europe, where they use acceleration sensor and gyroscope to measure lateral acceleration and roll velocity of the vehicles [8]. And through the control signal transmitted by the sensor, the electrical mechanical actuators will make necessary adjustments for tilting of the train.

2.3 Inertia Measurement System

For the determination of orientation movement acting upon a single object, typically a combination of gyro sensor and accelerometer had being used. It is also commonly known as a single unit called Inertia Measurement Unit (IMU). This system had been widely used in different field of applications, including motion control on self-balancing robot and human airbag fall protection system [9, 10]. Besides, it also plays an important role for applications on dynamic orientation calculation in Inertia Navigation System (INS) and Altitude and Heading Reference System (AHRS), where they have being commonly used in military vehicles, such as aircraft, submarines, missiles and spacecraft [4, 9]. Together with IMU sensors, both of these systems are used to provide inertial measurement and position guidance to the operator without the need to communicate with satellite.

A simple design of an IMU typically incorporates both accelerometer and gyro sensor in a single circuit platform. The angular velocity (ω) of a moving object could be measured from a gyro sensor [4, 9-11]. However, in order to obtain the tilt angle(θ), integration of the collected data is required as shown in the equation below:

$$\theta = \int \omega dt \quad (1)$$

Despite that, one of the main problems associated with gyro sensor is the so called, drifting error, where the output is not constant offset even when the object

is at rest. Hence, this small error or noise could incur serious problem where the integration of the results will diverge to infinity [9]. In order to compensate this angular drift, accelerometer is commonly integrated together with gyro sensor. It is mainly used to measure the motion and gravitational acceleration acting upon an object. The tilt angle of an object can also be measured and calculated with an accelerometer, as shown in the equation below:

$$\theta = \sin^{-1} \frac{\textit{Measured Acceleration}}{\textit{Gravity Acceleration}} \quad (2)$$

However, similar to the problem faced by solely using gyroscope, accelerometer also encountered with the inaccuracy of measurement data. For the case of an moving object, there will be a number of extra components of acceleration induces on it, other than the constant acceleration due to earth's gravity [4]. Although these additional forces and error might only occur at a certain period, however it could also results in inaccurate tilting angle, especially for applications which requires high accuracy. Some of the method to minimize this effect includes introduction of low-pass filter to the output of accelerometer [4, 9-12]. Although it might slow down the process time of the data, however it could increase the accuracy by eliminating any unwanted high frequency of forces components.

Hence, the combination of gyro sensor and accelerometer in a single unit could be used to compensate the error occurred between both of them, where the gyro sensor is more suitable for short term usage and accelerometer is more useful for long term [4]. In order to effectively combine the processed data from both of the sensor unit, Kalman or complementary filter is typically designed and used [4, 9, 11-12]. Both of these filters will reduce the drifting error and produce accurate tilt angle in a shorter period of time, by continuously update and correct the measurement. In addition to that, a number of manufacturers have also included magnetometer, low-noise amplifier and digital filter to increase the sensitivity and accuracy of the whole measurement unit. However, it might incur more cost to the development of the measurement unit and might lead to very complex interfacing and control algorithm.

CHAPTER 3

METHODOLOGY

3.1 Overview

A combination of motion sensor devices mainly consisting of MEMS-based gyroscope and accelerometer are used throughout the project. Both of these sensors are capable of measuring the orientation movement of an moving object, where a tri-axis angular rate gyros are capable of detecting the roll, yaw and pitch angles, while an accelerometer will detect the acceleration with respect to x, y and z-axis, as shown in Figure 3. An IMU that combine both of these sensor devices is a suitable candidate for motion detection and recording for our application. A low-cost Arduino IMU distributed by Cytron, was served as the key component of the prototype. It is equipped with MPU6000 3-axis accelerometer and gyroscope, that has the capabilities of measuring up to a limit of $\pm 16g$ of force acceleration and gyro sensitivity of up to 131 LSBs/dsp Onboard Arduino ATmega328 processor and A/D Converter continually access and read data from the sensor device via Serial Peripheral Interface (SPI). A simple flow of the prototype is shown in Figure 4.

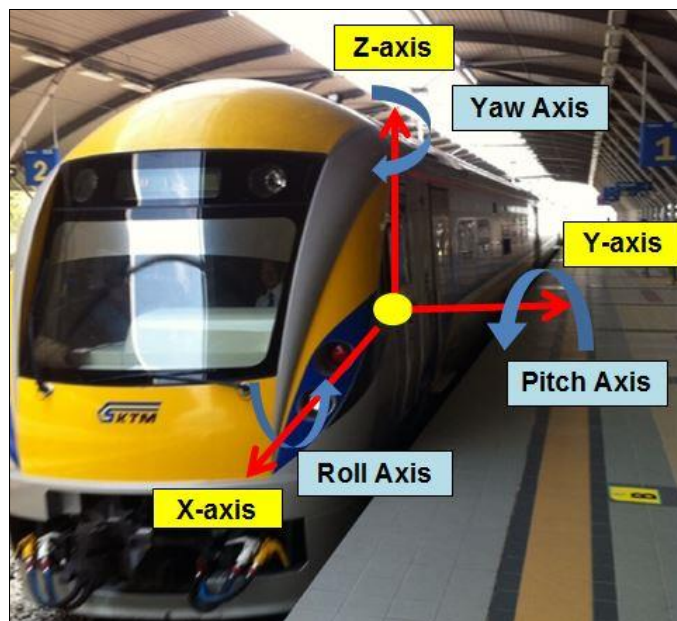


Figure 3. Illustration of axis orientation on train.

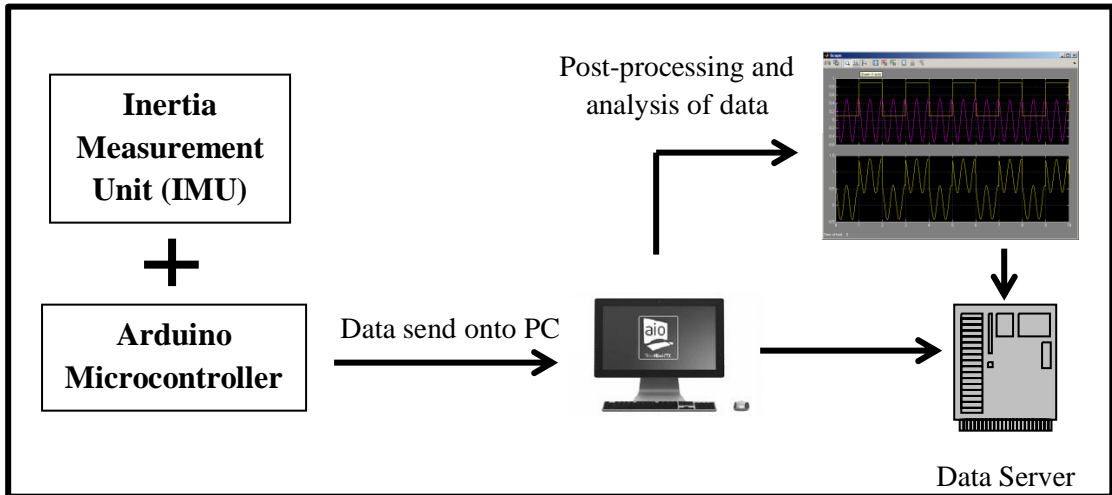


Figure 4. Simple flow diagram on the overall setup of the project.

3.2 Experimental Setup

To verify the feasibility and applicability of the prototype, it is initially tested along a bumpy road in front of Chancellor Hall, UTP. Then, it will be conducted on passenger cabin of train services of Malaysia, to measure actual track features on a loaded and normal train operation. The primary route of consideration is the operation of Electric Train Services (ETS) from Kampar Station to KL Sentral Station. The key milestones of this project mainly separated into two stages, as shown in Figure 5. Gantt Chart was also showed as in Table 1.

Key Milestones	
First Stage	Second Stage
<input type="checkbox"/> Interfacing of Inertia Measurement Unit (IMU) onto PC <input type="checkbox"/> Verify prototype and actual data recording	<input type="checkbox"/> Data processing through MATLAB <input type="checkbox"/> Display and predict possible misalignment

Figure 5. Key Milestones of this project.

Table 1. Gantt Chart of the project.

Main Task	First Semester / Week														Second Semester / Week													
	1	2	3	4	5	6	7	8	9	10	11	12	13	14	1	2	3	4	5	6	7	8	9	10	11	12	13	14
• Literature Review	█	█	█	█																								
• Identify suitable hardware and purchasing				█	█	█	█																					
• Extended Proposal						●																						
• Assembly and initial testing								█	█	█																		
• Proposal Defence								●	●																			
• Hardware setup and testing								█	█	█	█																	
• Programming through Arduino IDE										█	█	█	█	█	█	█	█											
• Prototype calibration & experimental testing															█	█	█	█										
• Interim Report													●	●														
• Data collection																	█	█	█	█								
• Progress Report																					●							
• Data processing																	█	█	█	█	█	█						
• Project Dissertation and Presentation																							●	●	●	●	●	

3.3 Hardware Setup

In accordance with the given budget, the Arduino IMU was purchased with the amount of RM430.00 from Cytron Technologies Sdn. Bhd., which equipped with MPU-6000 device that includes tri-axis gyros and tri-axis accelerometer, HMC-5883L device with I2C magnetometer and Arduino ATmega328 microcontroller running at clock frequency of 16MHz. In addition to that, it also has a GPS port with FTDI autoswitch, which would allow additional GPS module to be installed. Other than that, an USB-to-UART converter was also purchased to facilitate the serial communication between PC and microcontroller.

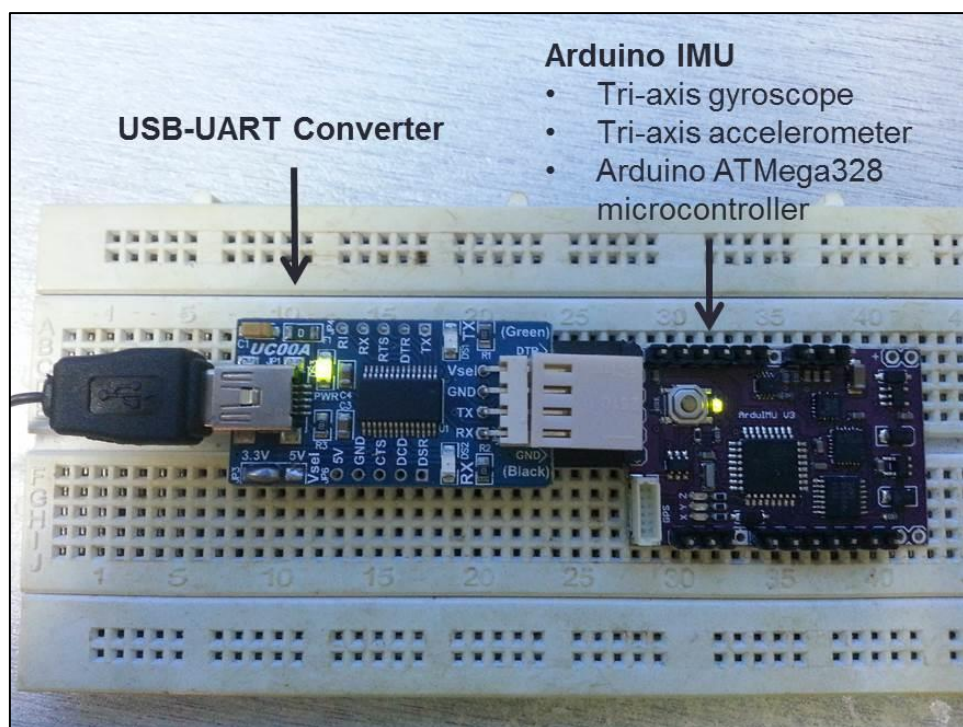


Figure 6. Connection between Arduino IMU and USB-UART Converter.

To connect the IMU with USB-UART converter, both units have to be soldered with 6-pins header socket. The 'Vsel' pin of USB-UART converter was also solder with 3.3V jumper to the middle pad and it could supply the rated voltage as the input to the IMU, where the Arduino Atmega328 could support input voltage from 1.8V to 5.5V. The connection table for both units was showed in Table 2.

ArduIMU	USB-UART Converter
Auto-reset	Data Terminal Ready (DTR)
Transmitter (Tx)	Receiver (Rx)
Receiver (Rx)	Transmitter (Tx)
Input Voltage	Voltage (Vsel)
Ground (GND)	Clear to Send (CTS)
Ground (GND) - BLK	Ground (GND)

Table 2. Connection table between ArduIMU and USB-UART Converter.

3.4 Hardware-Software Interface

As the Arduino Atmega328 was pre-loaded with Arduino Bootloader, the interfacing between IMU and PC could be programmed using Arduino IDE. The driver for USB-UART converter was successfully installed on PC and shown on USB Serial Port. A pre-defined library for MPU-6000 (gyro and accelerometer) was also added into Arduino IDE and programmed to obtain raw data from both sensors. A sample of display raw data from both gyro and accelerometer was shown in serial monitor, as in Figure 7. AN0 to AN2 represent data from gyroscope and AN3 to AN5 represent data from accelerometer, in x-axis, y-axis and z-axis, respectively. The device was placed in a reasonably flat surface and baud rate was set at 38400. By using Serial Peripheral Interface (SPI), the analog data from these sensors were sent at the clock rate of 1MHz and sample rate of about 50Hz. The program flow chart was shown as in Figure 8.

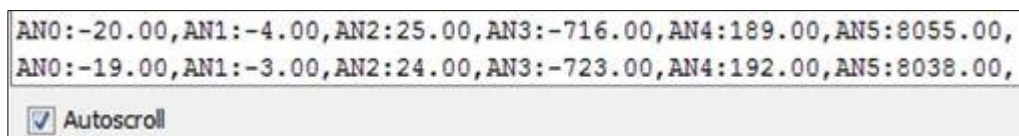


Figure 7. An example of analog data from gyroscope and accelerometer shown on serial monitor.

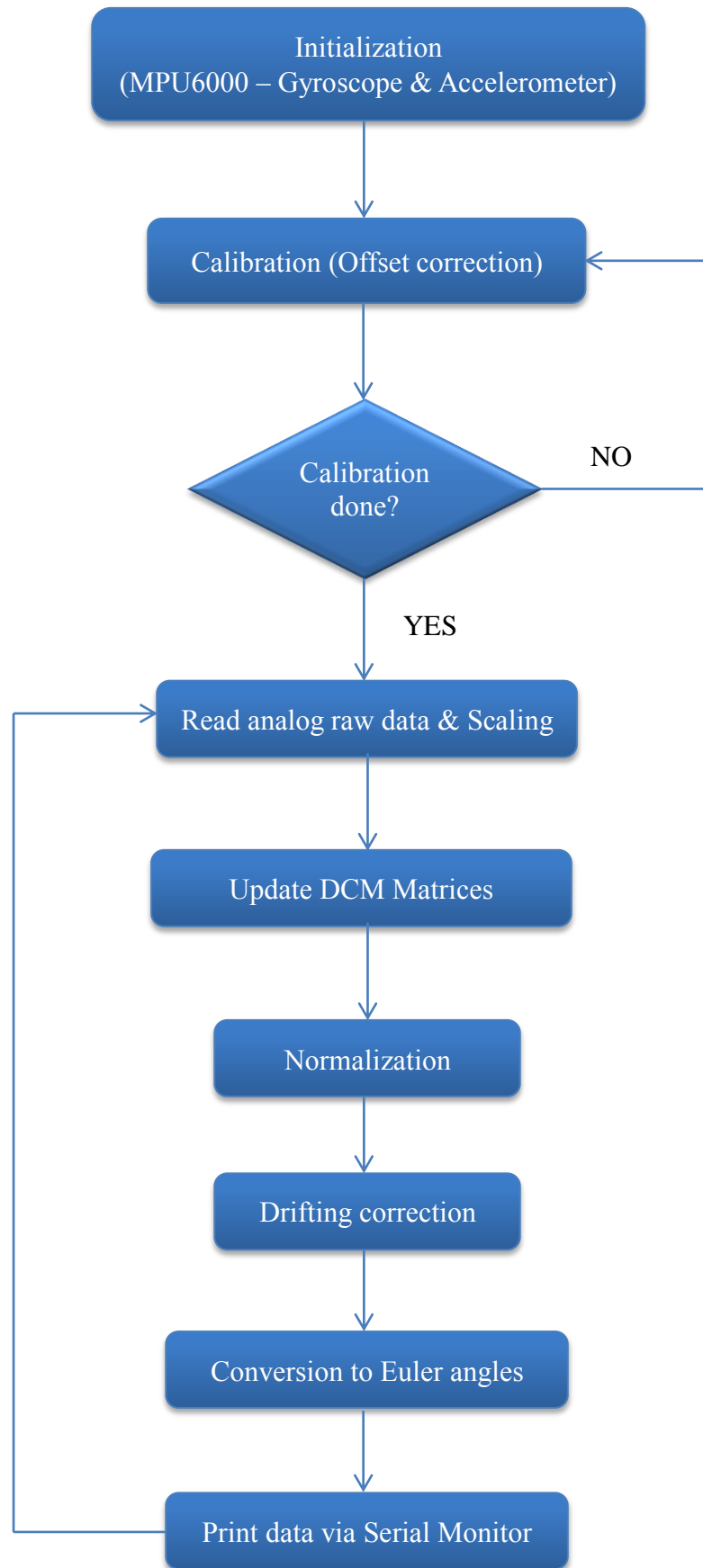


Figure 8. Program flowchart representing the workflow of interfacing between PC and IMU.

3.5 Direction-Cosine-Matrix (DCM) Algorithm

In order to obtain useful orientation movement from these analog raw data, a direction-cosine-matrix (DCM) algorithm was implemented in Arduino IDE. The block diagram of DCM algorithm was shown in Figure 9. The gyroscope was used as the primary source of orientation information. Reference vectors from accelerometers were used to detect gyro drifting and numerical error. A proportional plus integral (PI) feedback controller was implemented to feed back and make necessary adjustment to the data matrix in DCM.

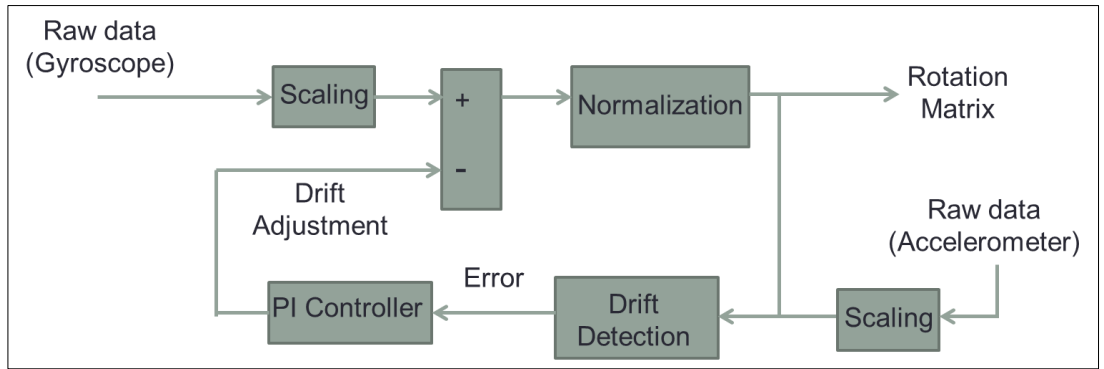


Figure 9. Block diagram of direction-cosine-matrix (DCM) algorithm.

To represent the orientation of moving train with respect to the ground frame, this DCM algorithm uses 9 elements of rotation matrix to describe the orientation of one coordinate system with respect to another. And, the key properties of the rotation matrix is orthogonality, where two vectors (body and ground coordinates) are perpendicular in every frame of reference. Hence, the row and columns are supposed to be perpendicular to each other and the sum of the squares of the elements in each column or row is equal to 1. A rotation matrix is shown in Equation (3). The acceleration motion on the train are represented as r_x , r_y and r_z (m/s^2) for all three axes while the gyroscope scaled data are labeled as G_x , G_y and G_z in radians per second.

$$Rotation\ Matrix = \begin{bmatrix} r_{xx} & r_{xy}/G_z & r_{xz}/G_y \\ r_{yx}/G_z & r_{yy} & r_{yz}/G_x \\ r_{zx}/G_y & r_{zy}/G_x & r_{zz} \end{bmatrix} \quad (3)$$

As shown in Figure 9, after the collection of raw data from gyroscope, the values were scaled to radians per second by multiplying with a gain value of approximately 0.00106 radians per second. Meanwhile, the raw data from accelerometers were also scaled to m/s^2 by multiply with a gain value of approximately 417.533. These pre-determined values were obtained from DCM algorithm developed by J. Munoz and W. Premerlani [19]. From the rotation matrix created by both data from gyroscope and accelerometers, normalization process is required to maintain the orthogonality conditions as described in Equation (3). The orthogonality error value is calculated by the dot product of the X and Y rows of the matrix, as shown in Equation (4).

$$error = X.Y = X^T Y = [r_{xx} \quad r_{xy} \quad r_{xz}] \begin{bmatrix} r_{yx} \\ r_{yy} \\ r_{yz} \end{bmatrix} \quad (4)$$

After determining the orthogonality error, half of the error was apportion to each X and Y rows by using the formula show in Equation 5 and 6.

$$\begin{bmatrix} r_{xx} \\ r_{xy} \\ r_{xz} \end{bmatrix}_{orthogonal} = X_{orthogonal} = X - \frac{error}{2} Y \quad (5)$$

$$\begin{bmatrix} r_{yx} \\ r_{yy} \\ r_{yz} \end{bmatrix}_{orthogonal} = Y_{orthogonal} = Y - \frac{error}{2} X \quad (6)$$

The Z row of the rotation matrix is adjusted to be orthogonal to the X and Y row, by using the cross product of the X and Y rows as shown in Equation 7.

$$\begin{bmatrix} r_{zx} \\ r_{zy} \\ r_{zz} \end{bmatrix}_{orthogonal} = Z_{orthogonal} = X_{orthogonal} \times Y_{orthogonal} \quad (7)$$

The last step in the normalization process is to scale the rows of the rotation matrix to adjust the magnitude of each row vector to one. The formula used for scaling in X-row is shown in Equation 8 and the same applied to Y and Z-rows.

$$X_{normalized} = \frac{1}{2} (3 - X_{orthogonal} \cdot X_{orthogonal}) X_{orthogonal} \quad (8)$$

For drifting adjustment, the reference vector from accelerometers were used to detect gyro drifts and provide a negative feedback loop back to the gyros to make any necessary adjustment. From DCM algorithm, the orientation error is calculated by taking the cross product of the measured vector with the vector estimated by the direction cosine matrix, as shown in Equation 9.

$$error_{roll,pitch} = Acceleration_x \times r_{zx} \quad (9)$$

A proportional plus integral (PI) feedback controller is then used to produce a rotation rate adjustment for the gyroscope. The K_p and K_i terms were taken as 0.015 and 0.000010, respectively, as developed by J. Munoz and W. Premerlani [19]. The output from PI controller is then fed back to scaled gyro signals.

Based on the rotation matrix created, the Euler angles can then be calculated based on the formula shown in Equation 10, 11 and 12.

$$Pitch = - \sin^{-1} r_{zx} \quad (10)$$

$$Roll = atan2 (r_{zy}, r_{zz}) \quad (11)$$

$$Yaw = atan2 (r_{yx}, r_{xx}) \quad (12)$$

CHAPTER 4

RESULTS AND DISCUSSION

4.1 Output Data

With the implementation of DCM algorithm, the output data in terms of Euler angles were tested at different angles and axis. However, the primary consideration was taken at roll and pitch angles, which would be useful to predict the turn rate of the train along its track while supported by data from tri-axis acceleration. The samples of output data with and without DCM algorithm were shown in Figure 10.

(i) At reasonably flat surface (0°)

(a) Uncorrected data with drift error

ROLL:-11.20,	PITCH:-59.28,	YAW:18.74,	ACC_X:-0.21,	ACC_Y:0.22,	ACC_Z:9.43,
ROLL:-11.27,	PITCH:-59.32,	YAW:18.81,	ACC_X:-0.13,	ACC_Y:0.21,	ACC_Z:9.49,
ROLL:-11.32,	PITCH:-59.36,	YAW:18.85,	ACC_X:-0.17,	ACC_Y:0.18,	ACC_Z:9.47,
ROLL:-11.40,	PITCH:-59.47,	YAW:18.91,	ACC_X:-0.19,	ACC_Y:0.21,	ACC_Z:9.49,
ROLL:-11.50,	PITCH:-59.71,	YAW:19.01,	ACC_X:-0.15,	ACC_Y:0.22,	ACC_Z:9.49,
ROLL:-11.62,	PITCH:-59.97,	YAW:19.12,	ACC_X:0.06,	ACC_Y:0.20,	ACC_Z:9.50,
ROLL:-11.65,	PITCH:-59.97,	YAW:19.15,	ACC_X:-0.10,	ACC_Y:0.20,	ACC_Z:9.49,
ROLL:-11.68,	PITCH:-59.96,	YAW:19.18,	ACC_X:-0.21,	ACC_Y:0.22,	ACC_Z:9.54,
ROLL:-11.80,	PITCH:-60.21,	YAW:19.28,	ACC_X:-0.05,	ACC_Y:0.23,	ACC_Z:9.49,
ROLL:-11.89,	PITCH:-60.39,	YAW:19.36,	ACC_X:-0.16,	ACC_Y:0.26,	ACC_Z:9.43,

Autoscroll

(b) Corrected data with DCM algorithm

RoLL:-0.05,	PITCH:-0.07,	YAW:0.29,	ACC_X:0.02,	ACC_Y:-0.04,	ACC_Z:9.47,
RoLL:-0.05,	PITCH:-0.07,	YAW:0.29,	ACC_X:0.04,	ACC_Y:-0.04,	ACC_Z:9.46,
RoLL:-0.06,	PITCH:-0.08,	YAW:0.29,	ACC_X:0.01,	ACC_Y:-0.00,	ACC_Z:9.51,
RoLL:-0.06,	PITCH:-0.08,	YAW:0.29,	ACC_X:0.03,	ACC_Y:-0.01,	ACC_Z:9.53,
RoLL:-0.06,	PITCH:-0.08,	YAW:0.29,	ACC_X:-0.02,	ACC_Y:0.01,	ACC_Z:9.50,
RoLL:-0.06,	PITCH:-0.07,	YAW:0.29,	ACC_X:0.03,	ACC_Y:0.02,	ACC_Z:9.49,
RoLL:-0.05,	PITCH:-0.08,	YAW:0.29,	ACC_X:-0.00,	ACC_Y:0.01,	ACC_Z:9.49,
RoLL:-0.05,	PITCH:-0.08,	YAW:0.29,	ACC_X:0.01,	ACC_Y:-0.01,	ACC_Z:9.55,
RoLL:-0.05,	PITCH:-0.08,	YAW:0.29,	ACC_X:-0.01,	ACC_Y:-0.04,	ACC_Z:9.51,
RoLL:-0.05,	PITCH:-0.07,	YAW:0.29,	ACC_X:0.01,	ACC_Y:-0.00,	ACC_Z:9.48,

Autoscroll

Figure 10. Uncorrected and corrected output data when IMU placed on a reasonably flat surface.

It should be noted as in Figure 10 (a), the Euler angles in terms of roll, pitch and yaw orientation shows a higher variation as compared to corrected data with accelerometer through DCM algorithm. Also, the increment of three Euler angles for each axis could be due to accumulation of numerical and drift error, which caused the uncorrected Euler angles grow to infinity. Meanwhile, for the corrected data, the roll angle varies between offset values of around $\pm 0.06^\circ$ while the pitch angle varies between approximately $\pm 0.08^\circ$. As the yaw orientation requires reference data from external GPS module or magnetometer for drift cancellation, hence the yaw data in this DCM algorithm is yet to be corrected and it would not be suitable to predict misalignment of train track as it only signify the heading direction of the train. In resting position, acceleration in x and y-axis yields an offset value of approximately $\pm 0.04 \text{ m/s}^2$, while acceleration in z-axis produces an initial value of approximately 9.50 m/s^2 , with slight variation of $\pm 0.04 \text{ m/s}^2$.

(ii) Rotate to 45° along x-axis (Roll angle)

(a) Uncorrected data with drift error

ROLL:-65.92,	PITCH:-1.36,	YAW:-3.77,	ACC_X:0.32,	ACC_Y:-5.82,	ACC_Z:8.45,
ROLL:-66.19,	PITCH:-1.22,	YAW:-3.80,	ACC_X:0.26,	ACC_Y:-5.82,	ACC_Z:8.49,
ROLL:-66.26,	PITCH:-1.24,	YAW:-3.78,	ACC_X:0.25,	ACC_Y:-5.80,	ACC_Z:8.49,
ROLL:-66.15,	PITCH:-1.32,	YAW:-3.76,	ACC_X:0.24,	ACC_Y:-5.75,	ACC_Z:8.49,
ROLL:-66.31,	PITCH:-1.29,	YAW:-3.76,	ACC_X:0.24,	ACC_Y:-5.81,	ACC_Z:8.52,
ROLL:-66.39,	PITCH:-1.31,	YAW:-3.77,	ACC_X:0.16,	ACC_Y:-5.74,	ACC_Z:8.56,
ROLL:-66.65,	PITCH:-1.29,	YAW:-3.78,	ACC_X:0.20,	ACC_Y:-5.79,	ACC_Z:8.53,
ROLL:-67.15,	PITCH:-1.11,	YAW:-3.82,	ACC_X:0.25,	ACC_Y:-5.79,	ACC_Z:8.53,
ROLL:-67.02,	PITCH:-1.24,	YAW:-3.79,	ACC_X:0.21,	ACC_Y:-5.85,	ACC_Z:8.44,
ROLL:-66.87,	PITCH:-1.33,	YAW:-3.75,	ACC_X:0.24,	ACC_Y:-5.74,	ACC_Z:8.52,

Autoscroll

(b) Corrected data with DCM algorithm

RoLL:-49.20,	PITCH:0.04,	YAW:-0.79,	ACC_X:-0.04,	ACC_Y:-8.69,	ACC_Z:7.55,
RoLL:-49.21,	PITCH:0.05,	YAW:-0.79,	ACC_X:0.00,	ACC_Y:-8.68,	ACC_Z:7.60,
RoLL:-49.20,	PITCH:0.05,	YAW:-0.79,	ACC_X:0.01,	ACC_Y:-8.70,	ACC_Z:7.53,
RoLL:-49.20,	PITCH:0.05,	YAW:-0.79,	ACC_X:0.02,	ACC_Y:-8.67,	ACC_Z:7.51,
RoLL:-49.21,	PITCH:0.04,	YAW:-0.79,	ACC_X:-0.06,	ACC_Y:-8.70,	ACC_Z:7.58,
RoLL:-49.22,	PITCH:0.05,	YAW:-0.79,	ACC_X:0.00,	ACC_Y:-8.72,	ACC_Z:7.53,
RoLL:-49.23,	PITCH:0.05,	YAW:-0.79,	ACC_X:-0.01,	ACC_Y:-8.70,	ACC_Z:7.54,
RoLL:-49.23,	PITCH:0.05,	YAW:-0.79,	ACC_X:-0.02,	ACC_Y:-8.71,	ACC_Z:7.47,
RoLL:-49.23,	PITCH:0.05,	YAW:-0.79,	ACC_X:-0.06,	ACC_Y:-8.72,	ACC_Z:7.53,
RoLL:-49.23,	PITCH:0.06,	YAW:-0.80,	ACC_X:0.00,	ACC_Y:-8.66,	ACC_Z:7.55,

Autoscroll

Figure 11. Uncorrected and corrected output data when IMU rotate to approximately 45° along x-axis.

Other than that, the initial prototype has also being tested at approximately 45° along the x and y-axis for roll and pitch angle. The results were shown as in Figure 11 and 12. As the unit was rotated along the x-axis to 45°, the orientation should focus on measuring the roll angle, while pitch angle remains at its own axis. The uncorrected data produces a similar result as in Figure 10 (a), where the accumulation of numerical and drift error causes the uncorrected roll angle to drift away. Meanwhile, the roll angle for corrected data shows an offset value of approximately 4° from the actual angle. Similar results were observed when tilting it to another side, which yield positive roll angle.

(iii) Rotate to 45° along y-axis (Pitch angle)

(a) Uncorrected data with drift error

ROLL:-72.67,	PITCH:68.58,	YAW:-41.32,	ACC_X:-9.42,	ACC_Y:1.06,	ACC_Z:6.25,
ROLL:-72.83,	PITCH:68.51,	YAW:-41.35,	ACC_X:-9.56,	ACC_Y:1.04,	ACC_Z:6.18,
ROLL:-72.76,	PITCH:68.42,	YAW:-41.27,	ACC_X:-9.44,	ACC_Y:1.06,	ACC_Z:6.20,
ROLL:-72.58,	PITCH:68.36,	YAW:-41.28,	ACC_X:-9.48,	ACC_Y:1.04,	ACC_Z:6.01,
ROLL:-72.82,	PITCH:68.21,	YAW:-41.29,	ACC_X:-9.44,	ACC_Y:1.10,	ACC_Z:6.33,
ROLL:-73.27,	PITCH:68.53,	YAW:-41.49,	ACC_X:-9.45,	ACC_Y:1.06,	ACC_Z:6.19,
ROLL:-73.61,	PITCH:68.74,	YAW:-41.66,	ACC_X:-9.55,	ACC_Y:1.24,	ACC_Z:6.23,
ROLL:-73.59,	PITCH:68.63,	YAW:-41.58,	ACC_X:-9.37,	ACC_Y:1.12,	ACC_Z:6.35,
ROLL:-73.65,	PITCH:68.51,	YAW:-41.53,	ACC_X:-9.55,	ACC_Y:1.09,	ACC_Z:6.28,
ROLL:-74.18,	PITCH:69.05,	YAW:-41.88,	ACC_X:-9.48,	ACC_Y:0.60,	ACC_Z:6.26,

Autoscroll

(b) Corrected data with DCM algorithm

RoLL:-2.25,	PITCH:-48.61,	YAW:4.82,	ACC_X:8.53,	ACC_Y:-0.24,	ACC_Z:7.64,
RoLL:-2.24,	PITCH:-48.59,	YAW:4.83,	ACC_X:8.36,	ACC_Y:0.28,	ACC_Z:7.69,
RoLL:-2.16,	PITCH:-48.56,	YAW:4.84,	ACC_X:8.48,	ACC_Y:-0.48,	ACC_Z:8.10,
RoLL:-2.24,	PITCH:-48.51,	YAW:4.94,	ACC_X:8.56,	ACC_Y:-0.75,	ACC_Z:7.71,
RoLL:-2.32,	PITCH:-48.51,	YAW:5.00,	ACC_X:8.53,	ACC_Y:-0.20,	ACC_Z:7.54,
RoLL:-2.30,	PITCH:-48.52,	YAW:4.99,	ACC_X:8.55,	ACC_Y:-0.32,	ACC_Z:7.69,
RoLL:-2.31,	PITCH:-48.53,	YAW:4.99,	ACC_X:8.51,	ACC_Y:-0.36,	ACC_Z:7.50,
RoLL:-2.32,	PITCH:-48.53,	YAW:4.99,	ACC_X:8.44,	ACC_Y:-0.47,	ACC_Z:7.73,
RoLL:-2.34,	PITCH:-48.51,	YAW:4.99,	ACC_X:8.54,	ACC_Y:-0.17,	ACC_Z:7.57,
RoLL:-2.30,	PITCH:-48.52,	YAW:4.97,	ACC_X:8.49,	ACC_Y:-0.48,	ACC_Z:7.99,

Autoscroll

Figure 12. Uncorrected and corrected output data when IMU rotate to approximately 45° along y-axis.

In Figure 12, the IMU was rotated to approximately 45° along the y-axis and the pitch angle was measured in this case. Similarly, the drifting error yields a continuous increment of pitch angle, which varies largely with the actual angle. Implementation of rotation matrix in DCM algorithm reduces the drifting error in pitch angle and results a variation of approximately 3.5° from the actual tilting angle.

The accelerometer has also being programmed in order to change the scale of acceleration up to $\pm 2G$, $\pm 4G$, $\pm 8G$ and $\pm 16G$ for actual application and data collection on heavy objects, such as car and train. The force of acceleration could only support up to $\pm 1G$ by default. In addition to that, the verification on the applicability and feasibility were initially tested on car. Orientation information on a moving car, such as roll angle, pitch angle, horizontal and vertical acceleration were collected and analyzed.

4.2 Car-mounted Field Testing

The prototype was mounted beneath the passenger seat of a car and travel along the road in front of Chancellor Hall, UTP, as shown in Figure 13. This test aimed to evaluate the applicability of the car-mounted IMU for detecting bump on the road. The car was travelling at an average velocity of 20 km/h within a duration of 1 minutes 30 seconds, for a distance of approximately 0.5 km .



Figure 13. One of the bump as located in front of Chancellor Hall, UTP.

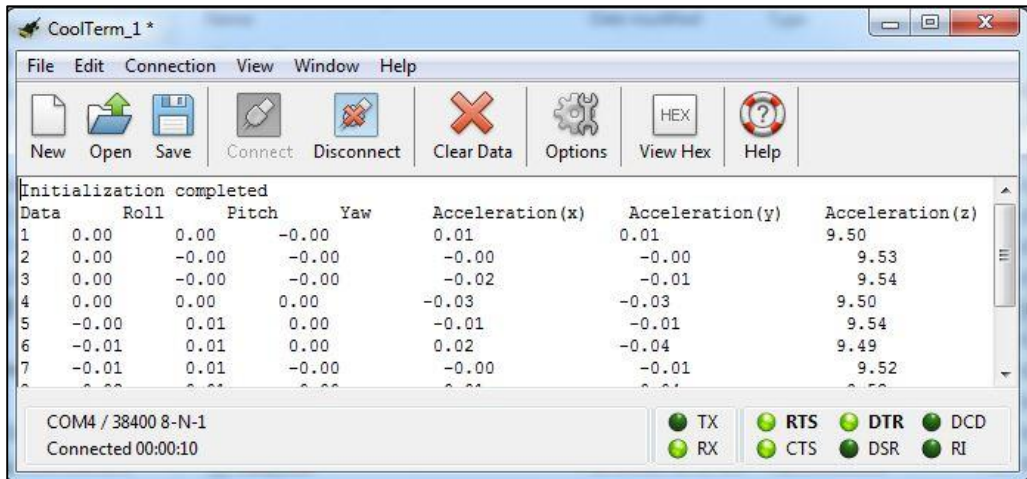


Figure 14. Display of measurement data on serial window.

The measurement data were serially sent onto PC and being captured by a serial terminal, known as ‘CoolTerm’, as illustrated in Figure 14. These collected data were saved into a text file and later being extracted into Excel and MATLAB for post-processing and analysis. Figure 15 and 16 showed the sample of captured data being stored in txt. (Text file) and xls. (Excel file) format. By saving all these data into the PC, it allows user to review and post-process the data. These data consists of Roll Angle($^{\circ}$), Pitch Angle($^{\circ}$) and Tri-axis acceleration(m/s^2). The travel distance for each data was estimated with assumption of constant velocity.

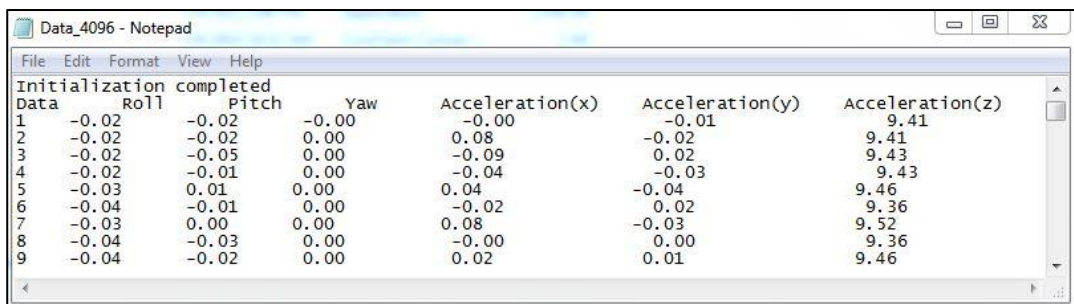


Figure 15. Measurement data in Text format.

	A	B	C	D	E	F	G	H	I
1	Initializati completed								
2	Data	Roll	Pitch	Yaw	Acceleration(x)	Acceleration(y)	Acceleration(z)	Distance (km)	
3	1	-0.02	-0.02	0	0	-0.01	9.41	0.00012	
4	2	-0.02	-0.02	0	0.08	-0.02	9.41	0.00024	
5	3	-0.02	-0.05	0	-0.09	0.02	9.43	0.00036	
6	4	-0.02	-0.01	0	-0.04	-0.03	9.43	0.00048	
7	5	-0.03	0.01	0	0.04	-0.04	9.46	0.0006	
8	6	-0.04	-0.01	0	-0.02	0.02	9.36	0.00072	
9	7	-0.03	0	0	0.08	-0.03	9.52	0.00084	
10	8	-0.04	-0.03	0	0	0	9.36	0.00096	
11	9	-0.04	-0.02	0	0.02	0.01	9.46	0.00108	
12	10	-0.03	-0.03	0	-0.04	-0.01	9.29	0.0012	

Figure 16. Measurement data in Excel file.

A total of approximately 4100 set of samples were collected and around 400 Kilobyte (KB) of data were saved onto PC. The system collects roughly about 30 sets of samples per second and sampling distance of between 110 *mm* to 125 *mm*. Figure 17. shows the overall collected data from car-mounted field testing which covers along a 0.5*km* distance with four separated bump as illustrated. As shown, these signals contain a certain degree of vibration noise, which could be due to the vehicle's suspension system, irregular running surfaces of vehicle and also sensor noise. The location of four bumps could be visually identified through pitch angle, x-axis acceleration and y-axis acceleration, where significant changes of magnitude and frequency could be observed. No significant observations were visually identified for roll and y-axis acceleration, due to different sources of noise present on the signal. On a later stage, a low-pass filter was used to improve signal to noise ratio and eliminate high-frequency noise, as the actual motion dynamics of vehicle are low compared to vibration and noise when it passes through an obstacle or bump.

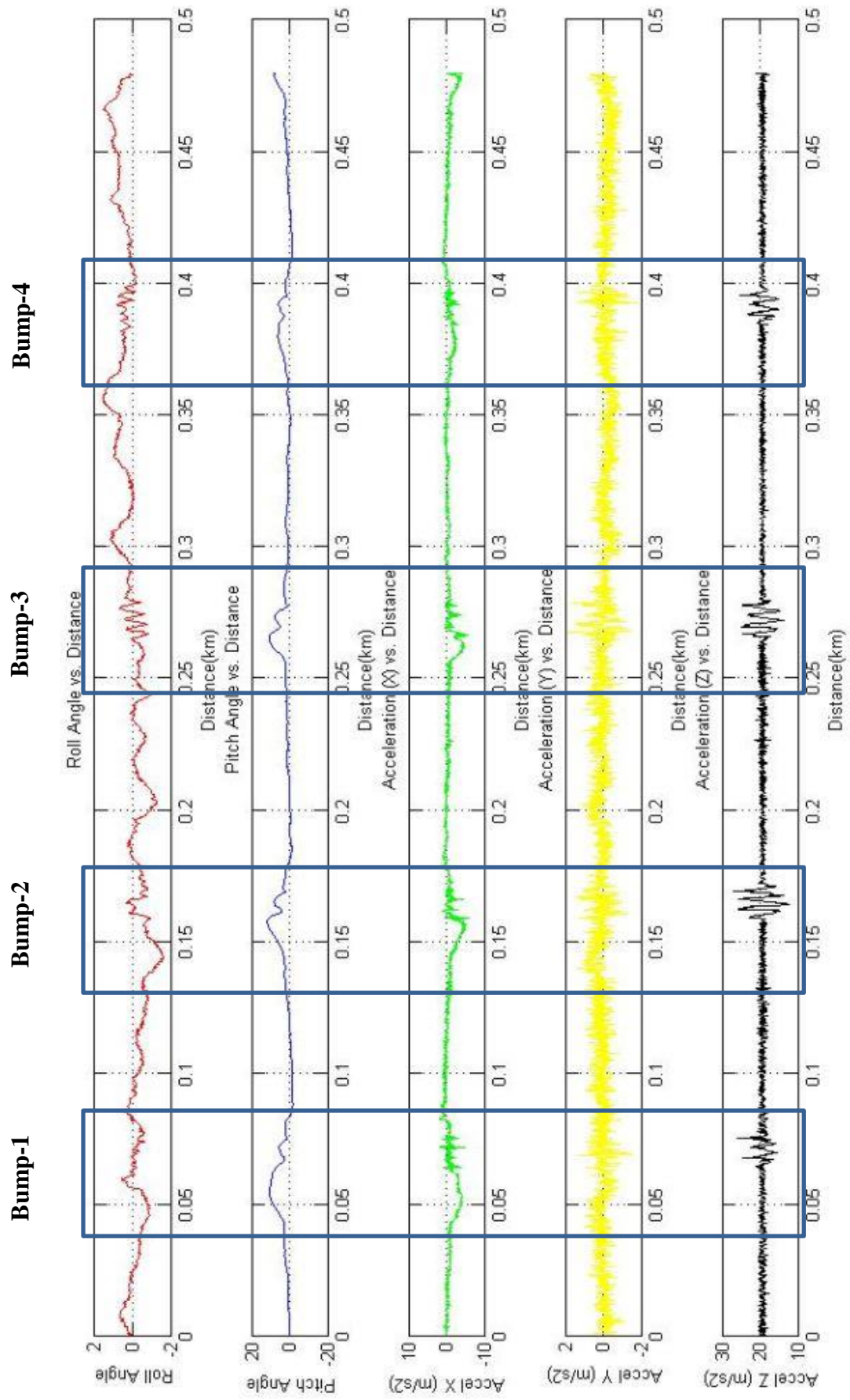


Figure 17. Collected IMU data for car-mounted field testing over distance

As shown in Figure 17, the vertical acceleration (z-axis) displayed higher sensitivity to the motion when it passes through the bump, where there is a significant change of frequency observed. Accelerations of the car can occur up to a maximum of 5.25 m/s^2 and up to 1.92 m/s^2 during deceleration upon reaching the bump. The maximum pitch angle is around 12° , when climbing up the bump. Concentrating on the intervals where it passes through second bump ($0.1 \text{ km} - 0.2 \text{ km}$) as shown in Figure 18, multiple spikes could be observed on x-axis acceleration when it passes over the bump and this could be due to motion distortion, where the acceleration in x-axis overflow and displace from its ground frame when passes through, thus causing it to record highly-susceptible value of acceleration and creates multiple spikes.

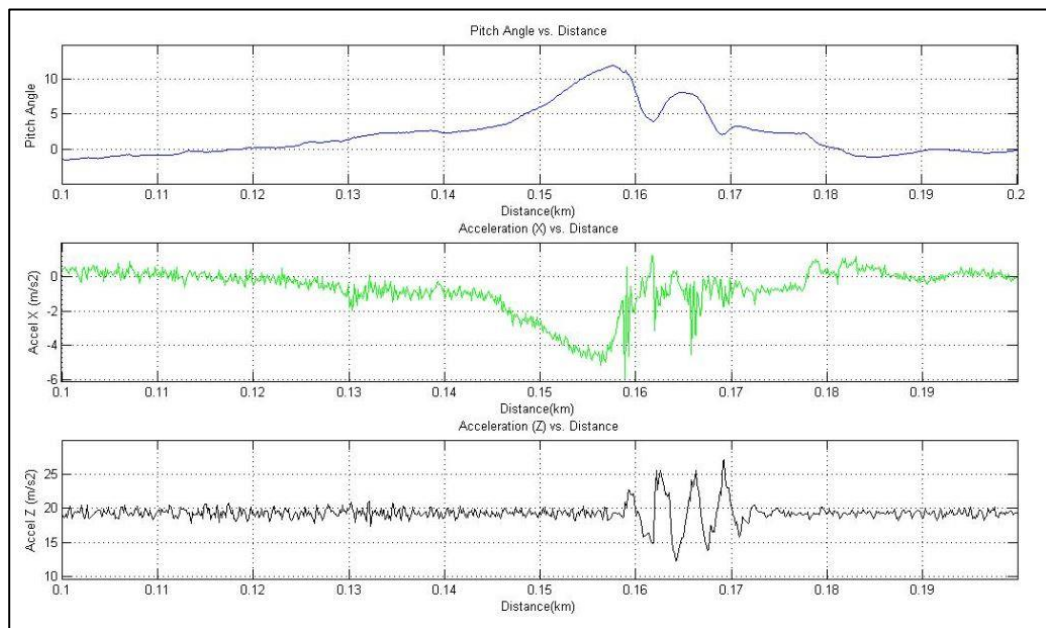


Figure 18. Close-up on pitch angle, x-axis acceleration and z-axis acceleration as car passes through second bump.

As the acceleration measurements contain vibrations from several sources, hence a low pass filter is used to improve signal to noise ratio. The filter used is a FIR (finite impulse response) filter with stopband frequency of 1 Hz. After filtering, car motion in terms of the roll angle and y-axis acceleration when it passes through the bump, could be more clearly identified as shown in Figure 19.

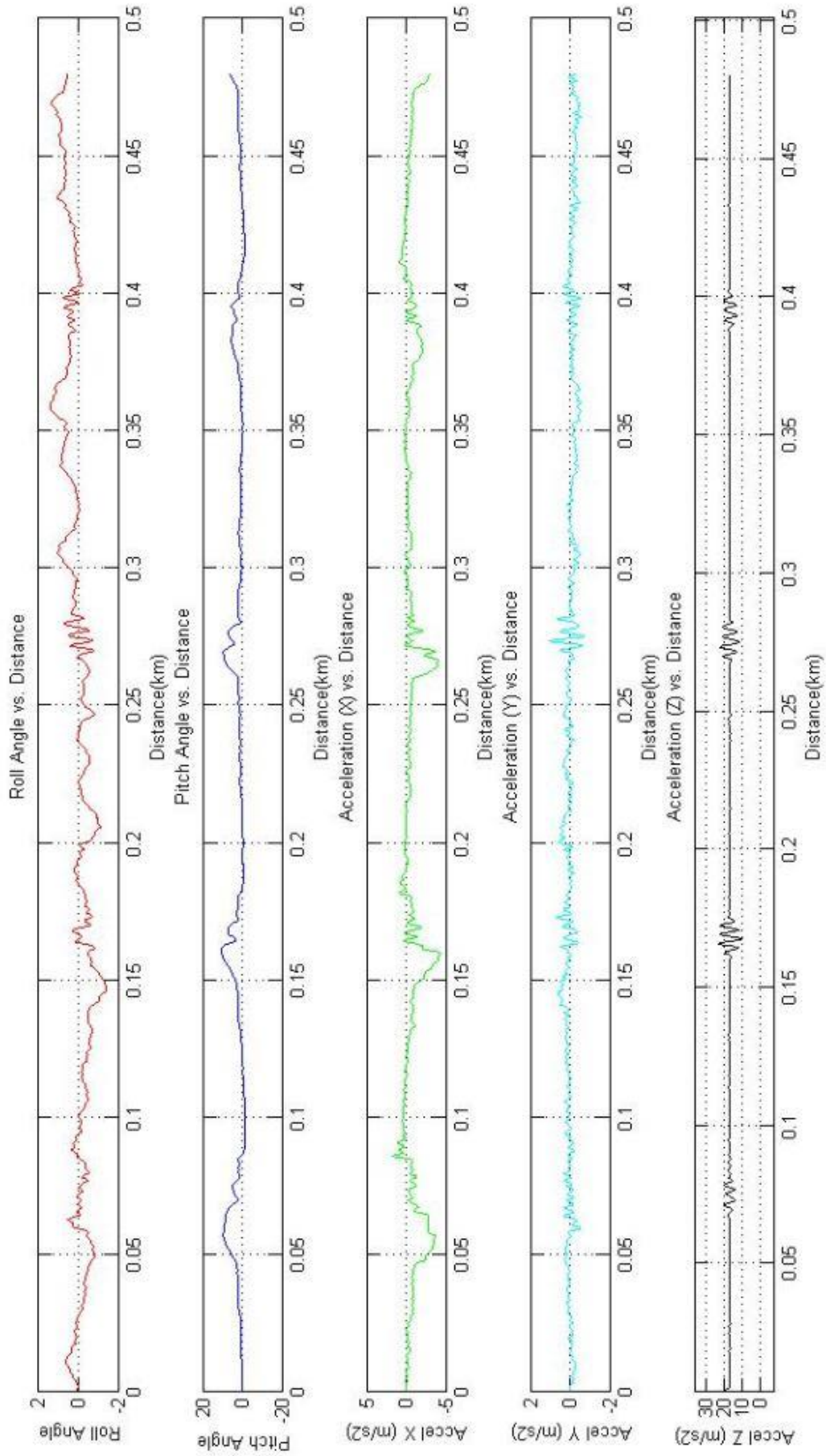


Figure 19. Collected IMU data with filtering for car-mounted field testing

As shown in Figure 19, filtering technique helps to improve the identification of car motion while eliminating vibration and noises, particularly for roll angle and y-axis acceleration which could be used to identify swinging motion of the car. It is believed that there are small variations of changes in terms of the swinging motion of the car when passing through the bump, however it was overthrown by noises and possibly by its suspension system, as shown in Figure 17. Low dynamics of car motion due to bumping surface could now be more easily identified, particularly improvement on roll angle and y-axis acceleration by eliminating high dynamics noise and vibration. These two data can then be included as a supporting data to identify condition of road surfaces. Hence, implementation of low-pass filter could help in better visualization and identification of uneven road surfaces. From the motion measurements, several road features could be extracted and these data showed good repeatability under same road condition.

4.3 Train-mounted Field Testing

The system was tested on a two direction inter-city train track of Electric Train Services (ETS) by Keretapi Tanah Melayu Berhad (KTMB). The field testing covered from Kampar Station to KL Sentral Station, which has a length of about 230 km. This route was chosen as it covers several railway environments, such as rural area, fast track section, tunnel and city station. A total of 9 stops were made along the journey. The electric train can speed up to a maximum of 140 km/h. The system was mounted and taped on the floor of the passenger cabin, which is near to the tail of the train. These data represent usual conditions of a normal operating and passenger-loaded train.

A total of 310,000 set of samples were captured and 36MB data were saved into PC via serial terminal. These data were captured with a sampling rate of about 707 mm – 734 mm. It is also estimated that approximately 30 sets of samples were collected per second. Figure 20 presents the collected data from Kampar Station to KL Sentral Station. The distances travelled were estimated based on assumptions that the train was travelled on constant velocity of 125km/h. The actual distance and location subject to correction through future expansion with additional GPS module.

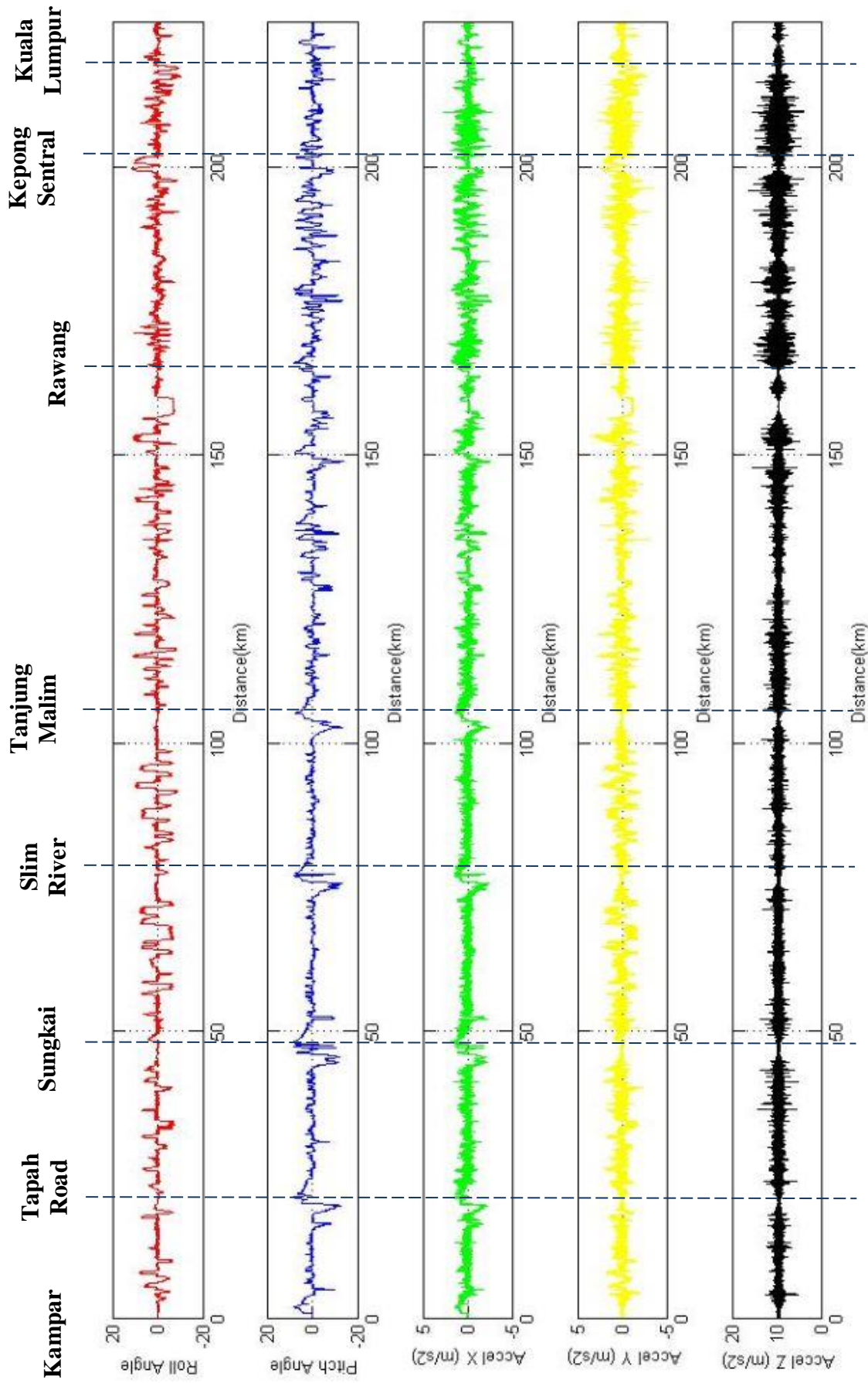


Figure 20. Collected IMU data for train-mounted field testing, covering from Kampar Station to KL Sentral Station

4.3.1 Overall Measurement Analysis

The on-board IMU was aligned based on the track feature in Kampar Station. Offset values were collected and calibration were done during initialization. Observing the overall motion data collected in Figure 20, vertical motion of the train could be visually analyzed through z-axis acceleration, where the most severe vertical acceleration were collected in city station, from Rawang Station to Kuala Lumpur Station (160 km – 220 km). The initial values of z-axis acceleration vary between 9.40 m/s^2 to 9.50 m/s^2 on even and smooth surfaces. However, it shows high magnitude changes in vertical acceleration near to Rawang Station and the acceleration variation could reached from a minimum value of 3.93 m/s^2 up to a maximum of 16.46 m/s^2 . Urban station such as Rawang, Kepong and Kuala Lumpur Station could suffer from severe and faulty track features due to heavy and rapid usage of passenger transport train as well as freight train. The train engine was running throughout the journey and switched off at the end of data collection in KL Sentral Station.

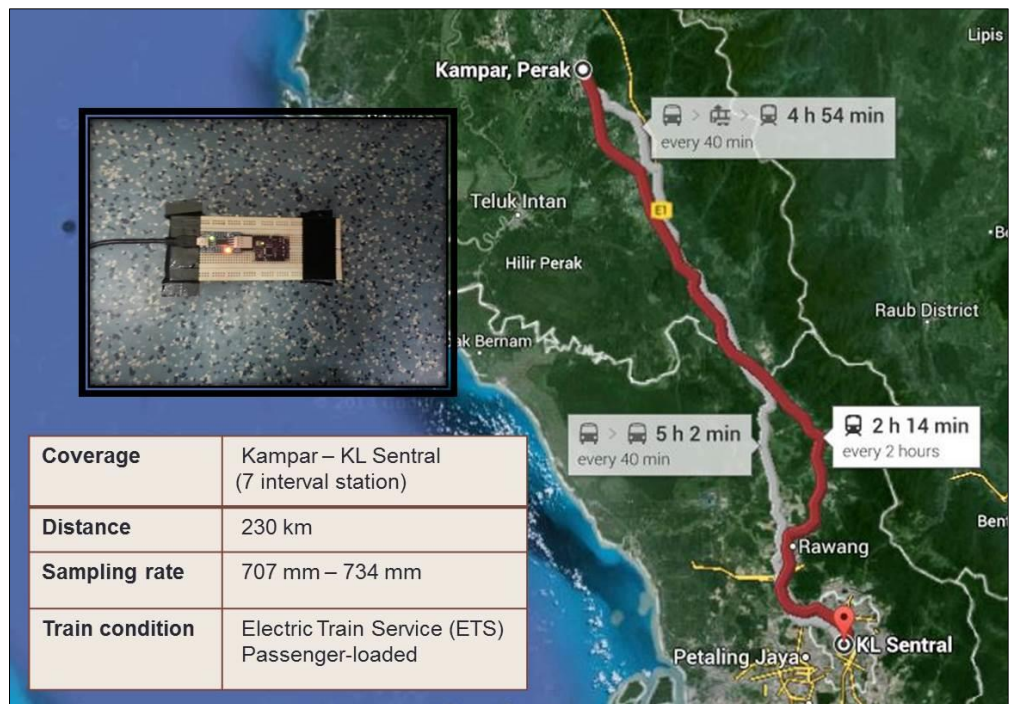


Figure 21. Distance coverage for train-mounted field testing. Picture inset shows the mounting of prototype on-board.

Meanwhile, the forward acceleration or deceleration of the train could also be observed through x-axis acceleration. A significant deceleration could be observed before the train approaching into every station, these values could reach up to 2.71 m/s^2 for deceleration. Similarly, forward acceleration of up to 2.70 m/s^2 was also observed when the train leaves the stopping station. The accelerating and decelerating motion of the train could also be supported by data from pitch angle. A pitch-down motion was observed when the train slows down before entering station platform, which results in negative pitch angle. Similar observation was seen as the train accelerates, which then lead to positive pitch angle. The swinging and rotating motion of the train could not be visually identified, as it also records the turn rates as the train passes through a curve. Similar to car-mounted field testing, acceleration in y-axis might overflow and saturate when the train travelling through banked curve, due to the migration from its ground frame.

4.3.2 Track Characteristics

These collected data showed close relation by mapping with actual track features, such as straight track and curvature. A straight track has zero curvature and often allows train to travels in a higher speed than banked curvature. A relatively high magnitude was observed near to a straight track section before Rawang Station. Fig. 22. shows the corresponding measurement data from z-axis acceleration in KM147.6 to KM148. As compared with its surrounding track environment, a higher magnitude changes in the vertical acceleration was observed within a distance of 70 meter. This occurrence could be due to small portion of uneven running surface on the rail, thus causing a significant bumping effect on the train.

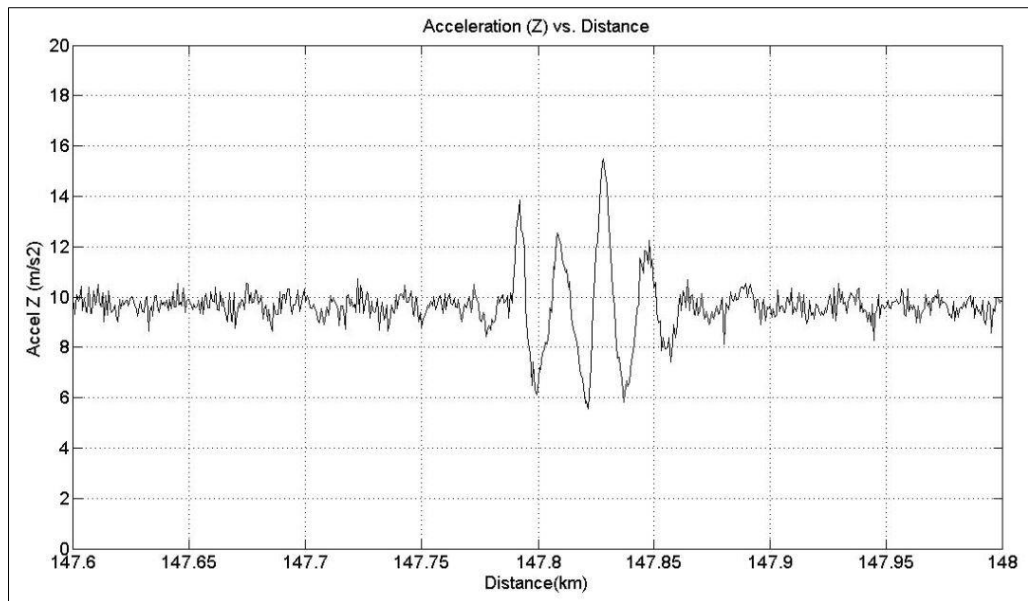


Figure 22. Vertical acceleration measurement in KM147.6 to KM148.

A banked curvature of a train track can be described as the lateral inclination of the train, due to one part of the track being higher than the other. It thus allows the train to travel at a higher speed through a curvature. Several curvatures were encountered in the experimental testing. It can be identified through a constant roll angle for a defined amount of time. However, as the train passes through these curvatures, the y-axis acceleration was observed to overflow and saturate at a constant value. Hence, the determination of train motion at curvature has to rely on its roll angle. Fig. 23. shows an example of measurement data in roll angles as it passes through two banked curvature. Roll angle as high as 9.8° was observed in the first curvature and follows by a relatively smooth straight track before transition onto second curvature. The limitation of roll angle on a non-zero curvature will ensure a smooth transition, safety and comfort to the passenger. Based on Fig. 22. and 23, a close-up on the accelerometer and gyroscope data showed that acceleration measurement contains motion vibration, as well as unwanted signals noise from ambient source. The gyroscope measurement are significantly unaffected by these noise and reflects only the train motion with small degree of sensor noise. This could be further supported by observation in their frequency spectrum. Although signal to noise ratio can be improved by using a low pass filter, however it is also

important to note that faulty track component and misaligned track section could impose high frequency component on the train and subsequently to the sensor unit.

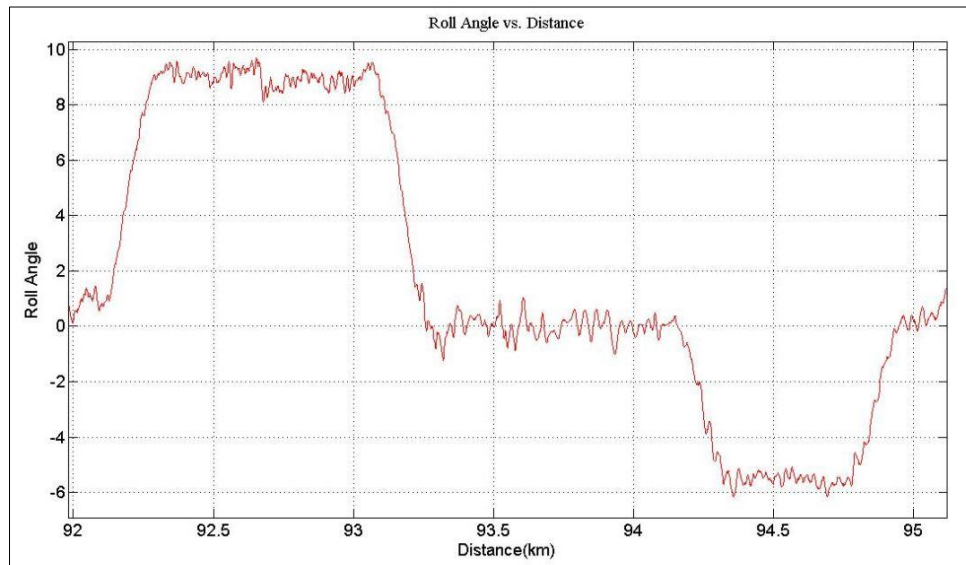


Figure 23. Roll angle measurement data corresponding to two banked curvature.

4.3.3 Frequency Spectrum

The frequency spectrum of the signal is visually represented by the spectrogram over its time signal. A short-time fourier transform (STFT) was performed with overlap method. Power spectral density (PSD) of each segment was also displayed on the spectrogram, represented by the degree of background colours. It can signify the dynamics of the train motion. Fig. 24. shows the frequency spectrum over time for y-axis acceleration measurement. Based on the spectrogram, it clearly separate the standing and moving motion of the train. Motion related to train movement has a dominant frequency between 0 – 3 Hz, based on the y-axis and z-axis acceleration spectrogram. The x-axis acceleration displays train motion at a slightly higher frequency, which is a result from untied mounting, thus causing noise on its axes. The plots also showed noise and vibrations with a dominant frequency of about 10 Hz. This unwanted signal could be a result from engine vibration and sensor noise, as it is present at almost every stopping motion of the train. Observing through the spectrogram of all three axes, a significant higher magnitude of frequency in z-axis acceleration

covering from Rawang to Kuala Lumpur Station (7500s – 10000s) was observed as shown in Fig. 25. Similar observation was also noted in y-axis acceleration.

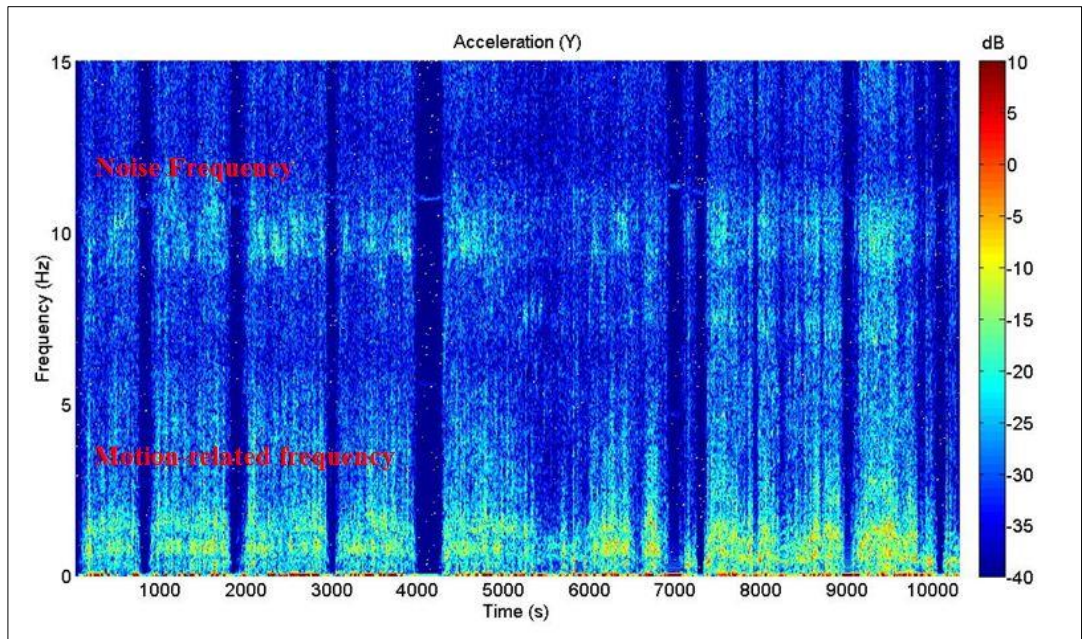


Figure 24. Frequency spectrum over time of Y-axis acceleration.

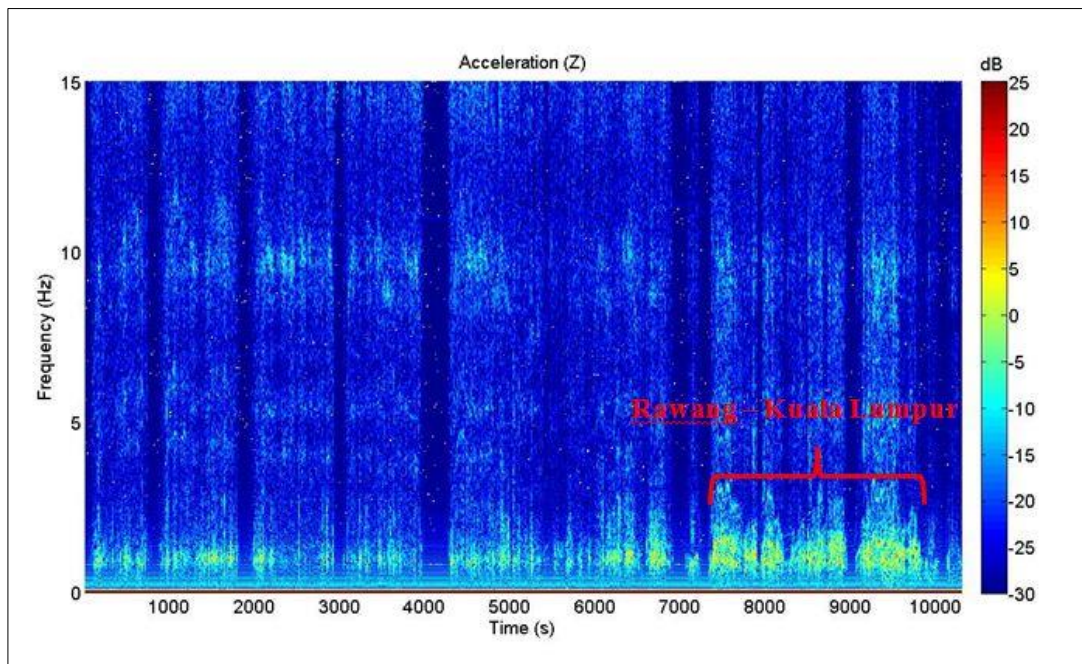


Figure 25. Frequency spectrum over time of Z-axis acceleration.

Both frequency spectrum of roll angle and pitch angle shows similar dominant frequency of 0 – 5 Hz for train motion. Meanwhile, these signals showed no evidence that it is affected by engine vibration. The spectrogram of roll angle can provide information related to the bank curvature and lateral movement of the train body. A significant high frequency of this signal could be due to instant rise of acceleration, resulting from laterally misaligned track. Meanwhile, the pitch angle provides information related to the accelerating and breaking period of the train. With focus on the roll angle and pitch angle, the faulty track components, such as ballast, switching gear and bottom plate could results in instant rise and vast vibration on the frequency spectrum of the orientation angle. Thus, these faulty track sections could be identified through the magnitude of its frequency spectrum due to increment in the irregularities between train and its track.

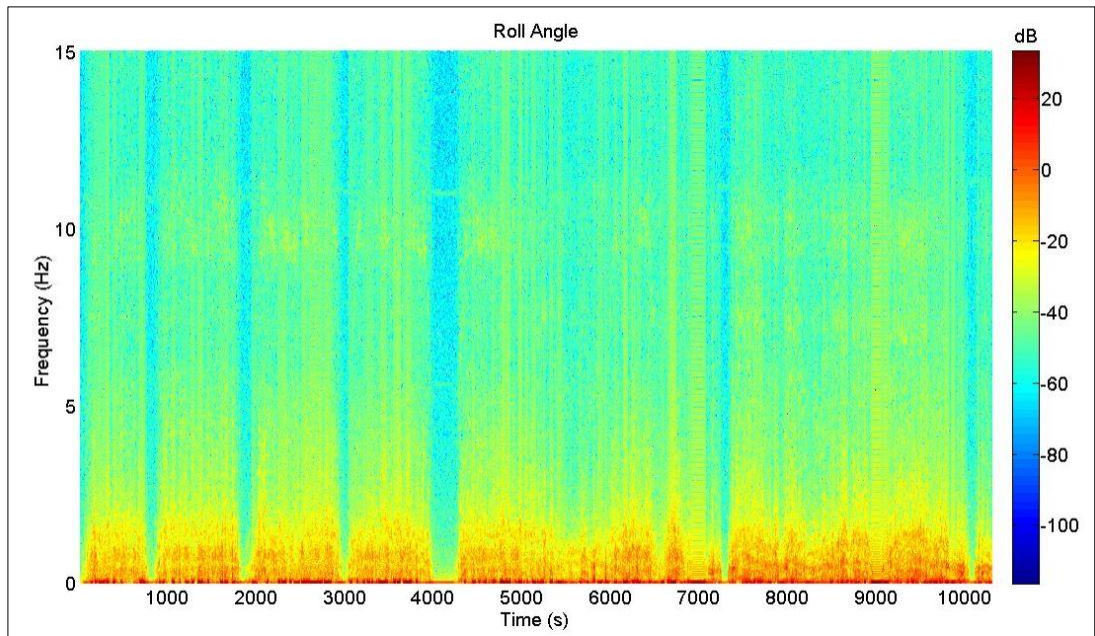


Figure 26. Frequency spectrum over time of roll angle.

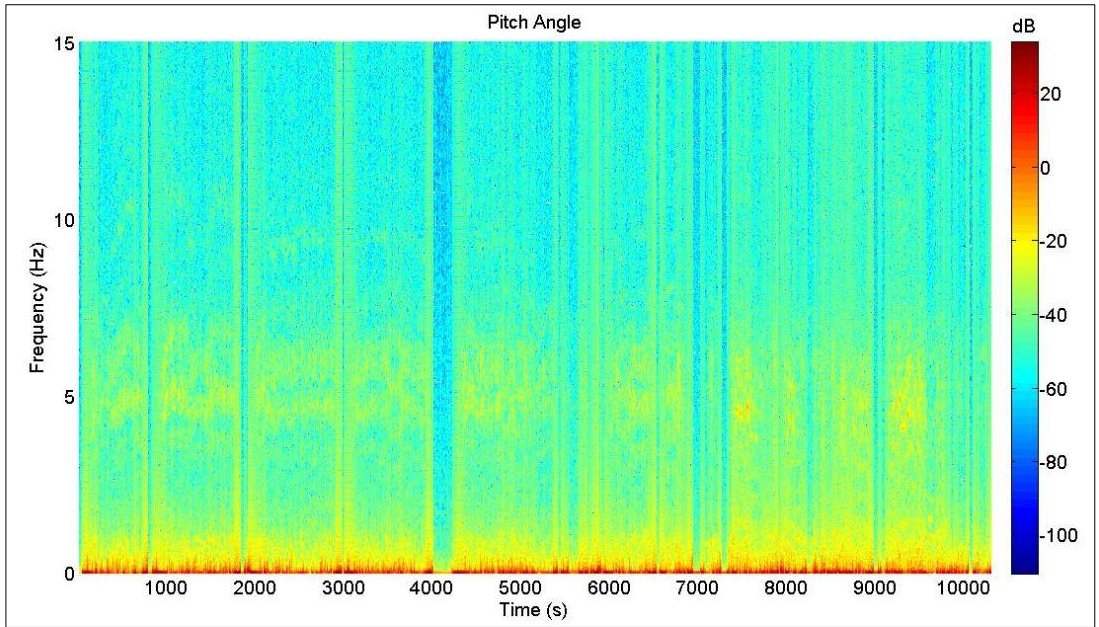


Figure 27. Frequency spectrum over time of pitch angle.

CHAPTER 5

CONCLUSION AND RECOMMENDATION

5.1 Conclusion

The development of train track misalignment detection system aims to provide feasible detection technique for any misaligned railways system, improves maintenance management and thus enhance riding comfort for passengers. In addition to that, the data collected from the interaction between train and its railway could also serves as one of the safety precaution for derailment or rollover. Train motion and orientation could be recorded by an IMU, which incorporated with gyroscope and accelerometer. Through Arduino microcontroller, the data collected from motion sensors can be transported to a PC for data collection and further processing. In order to increase the accuracy of these data, a DCM algorithm is required to compensate drifting error from gyro sensors based on reference data from accelerometer. The overall measurement analysis showed good correlation between actual track features and IMU sensor data. Several sources of unwanted vibrations and noise, such as engine, suspension, sensor placement has higher dominant frequency than low-dynamics train motion. Track features, such as bank curvature and straight track could be inferred from its measurement data. Analysis through the frequency spectrum over time provides insight onto possible misalignment region. The end product of this system is expected to be portable and used in a wide range of train vehicles, as it does not required any major installations and modifications to suit its usage.

5.2 Recommendations

To improve the feasibility and competitiveness of the system as a whole, a GPS mapping technique would also be an added advantage in order to display the actual location of train and provide reference data for yaw drift correction. Longitude and latitude position of the misaligned track surfaces could be provided to the maintenance team for inspection and repair work. However, several factors have to be made into consideration, including low accuracy due to atmospheric effect and geometric distribution of satellite. Further design improvement and optimization would be required for this add-on. Also, the IMU sensor can be mounted near to axle bearing to capture the direct interaction between wheels and its track. This method could help to reduce unwanted vibrations from its engine and suspension system. In addition to that, as the MEMS technology growing rapidly, these MEMS-based motion sensors could be expected to be fabricated and produced with a lower cost in the future. Hence, another possible improvement to this system would be to reduce its cost, without any trade-off for its accuracy and sensitivity. Design improvement to this system will also require detailed optimization on the placement of these sensors on the compartments, well-designed control algorithm and accurate sensor calibration.

REFERENCES

- [1] Train History. Types of Trains, Locomotives and Rails. [Online]. Available: <http://www.trainhistory.net/train-facts/train-types/>.
- [2] R. E. Risely, "Broken rail detector". United States of America Patent US3696243 A, 3 October 1972.
- [3] J. L. Davenport and D. L. Simard, "Sonic track condition determination system". United States of America Patent US 4932618 A, 12 June 1990.
- [4] W. W. Kong.(2009, May) Tutorials by Cytron Technologies. [Online]. Available: <http://tutorial.cytron.com.my/2012/01/10/measuring-tilt-angle-with-gyro-and-accelerometer/>.
- [5] R. Persson, "Tilting trains: Technology, benefits and motion sickness," Royal Institute of Technology, Stockholm, 2008.
- [6] L. Ren, Z. Jing and Z. Weihua, "Pantograph Dynamics and Control of Tilting Train," in *Proceedings of the 17th World Congress: The International Federation of Automatic Control*, Seoul, Korea, 2008.
- [7] Princeton Education. Tilting train. [Online]. Available: http://www.princeton.edu/~achaney/tmve/wiki100k/docs/Tilting_train.html.
- [8] Kable. Pendolino Tilting Train, Italy. [Online]. Available: <http://www.railway-technology.com/projects/pendolino-train/>.
- [9] J. Hau-Shiue and L. Kai-Yew, "Design and Control of a Two-Wheel Self-Balancing Robot using the Arduino Microcontroller Board," in *10th IEEE International Conference on Control and Automation (ICCA)*, Hangzhou, China, 2013.
- [10] S. Guangyi, C. Cheung-Shing, L. Yilun, Z. Guanglie, L. Wen J., L. Philip H. W. and L. Kwok-Sui, "Development of a Human Airbag System for Fall Protection using MEMS Motion Technology," in *Proceedings of the 2006 IEEE/RSJ: International Conference on Intelligent Robots and Systems*, Beijing, China, 2006.
- [11] L. Fanucci, A. Giambastiani, F. Iozzi, C. Marino, A. Rocchi, "Platform Based Design for Automotive Sensor Conditioning," in *Proceedings of the Design, Automation and Test in Europe Conference and Exhibition*, 2005.
- [12] F. Riewe, "Low-Cost Multiple Sensor Inertial Measurement System for Locomotive Navigation," Transportation Research Board of the National Academies, Washington DC, 1996.
- [13] J. R. Meyer, "Railroad radio frequency waveguide". United States of America Patent US 4207569 A, 10 June 1980.
- [14] J. J. Kuhn, "Dual signal frequency motion monitor and broken rail detector". United States of America Patent US 4306694 A, 22 December 1981.
- [15] T. R. Anderson, "Method and apparatus for detecting misaligned tracks". United States of America Patent US 6540180 B2, 1 April 2003.

- [16] J. Nielsen, E. Berggren, T. Lölgen, R. Müller, B. Stallaert and L. Pesqueux, "Overview of Methods for Measurement of Track Irregularities Important for Ground-Borne Vibration," International Union of Railways, 2013.
- [17] A. Drakopoulos and E. Ornek,, "Use of Vehicle-Collected Data to Calculate Existing Roadway Geometry," *Journal of Transportation Engineering*, vol. 126, pp. 154-160, 2000.
- [18] G. W. Roberts, X. Meng and A. H. Dodson, "Integrating a Global Positioning System and Accelerometers to Monitor the Deflection of Bridges," *Journal of Surveying Engineering*, vol. 130, pp. 65-72, 2004.
- [19] J. Munoz and W. Premerlani, "Direction Cosine Matrix IMU: Theory, " May, 2013.